Journal of Atmospheric and Oceanic Technology

Estimation of Rain Rate from PSD Airborne Doppler W-band Radar in CALWATER2

--Manuscript Draft--

Manuscript Number:	JTECH-D-17-0025
Full Title:	Estimation of Rain Rate from PSD Airborne Doppler W-band Radar in CALWATER2
Article Type:	Article
Corresponding Author:	Chris Fairall NOAA ESRL Boulder, UNITED STATES
Corresponding Author's Institution:	NOAA ESRL
First Author:	Chris Fairall
Order of Authors:	Chris Fairall
	Sergey Y. Matrosov
	Christopher R. Williams
	Edward J. Walsh
Abstract:	The NOAA Physical Science Division (PSD) W-band radar was deployed on a NOAA P-3D aircraft for 7 flights during a study of atmospheric rivers (AR's) associated with storm fronts off the US West coast in 2015 as part of the CALWATER2 field program. This paper presents an analysis of processing measured equivalent radar reflectivity factor (Zem) profiles to estimate precipitation rate based on attenuation of Zem due to absorption and scattering by raindrops at W-band. The first method uses the observed decrease of Zem with range below the aircraft to estimate column mean precipitation rates. The second method uses the difference in measured and calculated normalized radar cross section (NRCSm and NRCSc) retrieved from the ocean surface. Since NRCSc is fairly well-characterized as a function of wind speed and off-nadir angle, the difference (NRCSm - NRCSc) represents a total column attenuation estimate which yields a total column average rain rate estimate below the aircraft. These W-band radar retrieved rain rates are compared to estimates from two other systems on the P-3: a stepped frequency microwave radiometer (SFMR) and a wide swath radar altimeter (WSRA). We also compute mean profiles of Ze, rain drop gravitational fall velocity, rain attenuation, and precipitation rate in bins of rain rate. A method of correcting measured profiles of Zem for attenuation to estimate profiles of non-attenuated profiles of Ze is examined.
Suggested Reviewers:	

UNITED STATES DEPARTMENT OF COMMERCE
National Oceanic and Atmospheric Administration
Office of Oceanic and Atmospheric Research
Earth System Research Laboratory
325 Broadway – David Skaggs Research Center
Boulder, Colorado 80305-3337

February 3, 2017

Luca Baldini,
Italian National Research Council
Editor, Atmospheric Section
Journal of Atmospheric and Oceanic Technology
AMS

Dear Sir

I wish to submit the paper *Estimation of Rain Rate from PSD Airborne Doppler W-band Radar in CALWATER2* to JTECH. I will be corresponding author.

Regards,

Dr Chris Fairall
Team Lead: Boundary Layer Observations and Processes
David Skaggs Research Center
Boulder, CO 80305
E-mail: chris.fairall@noaa.gov
Phone: 303-497-3253

Click here to access/download

Cost Estimation and Agreement Worksheet

cwf_Cost Estimation and Agreement Worksheet.pdf

Estimation of Rain Rate from PSD Airborne Doppler W-band Radar in CALWATER2.

C.W. Fairall[1], SergeyY. Matrosov[1,2], Christopher R. Williams[1,2], E. J. Walsh[1]

[1]NOAA Earth System Research Laboratory, Physical Sciences Division

325 Broadway, Boulder, CO 80305-3337

[2]Cooperative Institute for Research in Environmental Sciences, University of Colorado, Boulder, CO

3 Feb 2017

Submission for Journal of Atmospheric and Oceanic Technology

Corresponding Author: C.W. Fairall, NOAA PSD, 325 Broadway, Boulder CO 80305, chris.fairall@noaa.gov, 303-497-3253

ABSTRACT

The NOAA Physical Science Division (PSD) W-band radar was deployed on a NOAA P-3D aircraft for 7 flights during a study of atmospheric rivers (AR's) associated with storm fronts off the US West coast in 2015 as part of the CALWATER2 field program. This paper presents an analysis of processing measured equivalent radar reflectivity factor (Z_{em}) profiles to estimate precipitation rate based on attenuation of Z_{em} due to absorption and scattering by raindrops at W-band. The first method uses the observed decrease of Z_{em} with range below the aircraft to estimate column mean precipitation rates. The second method uses the difference in measured and calculated normalized radar cross section ($NRCS_m$ and $NRCS_c$) retrieved from the ocean surface. Since $NRCS_c$ is fairly well-characterized as a function of wind speed and off-nadir angle, the difference ($NRCS_m - NRCS_c$) represents a total column attenuation estimate which yields a total column average rain rate estimate below the aircraft. These W-band radar retrieved rain rates are compared to estimates from two other systems on the P-3: a stepped frequency microwave radiometer (SFMR) and a wide swath radar altimeter (WSRA). We also compute mean profiles of Z_e, rain drop gravitational fall velocity, rain attenuation, and precipitation rate in bins of rain rate. A method of correcting measured profiles of Z_{em} for attenuation to estimate profiles of non-attenuated profiles of Z_e is examined.

1.0 **Introduction**

Precipitation is one of the most difficult and confounding meteorological variables to measure accurately and to sample sufficiently for meaningful averages. Most applications (e.g., hydrology, oceanic salinity budgets, global energy balances, soil moisture analysis) require grid-averaged precipitation rates. Because of the greatly patchy nature of precipitation, adequate sampling makes the use of surface-based conventional rain rates problematic. Ground-based scanning radars and satellite-borne radars can greatly improve sampling but introduce a host of accuracy issues (e.g., Lee and Zawadzki, 2006; Haynes et al. 2009). Two common issues with radar-based methods are the absolute calibration of the radar and the variation of radar-rain retrieval relationships with precipitation microphysics (Steiner et al. 2004; Lee and Zawadzki, 2006). Conventional raingauges have biases associated with wind effects on collection efficiency that are geometry dependent (Koschmeider 1934) and they provide an estimate for only rain rate. Disdrometers, which measure the rain drop size distribution (DSD) offer a superior surface characterization of precipitation microphysics because both rain rate, R, and equivalent radar reflectivity factor, Z_e, can be computed from the observations.

Whilst precipitation reaching the surface is the overarching variable in many weather application, precipitation formation processes are a critical research topic. Observational research into cloud/precipitation microphysical relationships has been dominated by airborne *in situ* DSD and ground-based mm-wavelength Doppler radar observing systems (Kollias et al., 2007). The advent of DSD and Doppler spectrum moment techniques (Frisch et al. 1995, 1998) increased the utility of remote-sensing methods which have subsequently expanded to a variety of approaches (including multi-wavelength, multi-Doppler peak, clear-air versus drop scattering modes; for more information, see Tridon et al. 2013, Williams 2016). Airborne mm-wavelength radars (Galloway et al., 1999) have greatly expanded the scope of radars to investigate the spatial distribution and vertical structure of precipitating cloud systems. One important weakness of moment-based methods in estimating precipitation rate is that the 0^{th}, 1^{st}, and 2^{nd} moments of the radar reflectivity-weighted Doppler velocity spectrum are essentially the 6^{th}, 7^{th}, and 8^{th} moments of the DSD for the Rayleigh-type scattering (see Eq. 9 in Frisch et al. 1995). Thus, radar moment methods may poorly constrain rain rate retrievals which is essentially the 3.67^{th} moment of the DSD. An independent constraint of one or more of the lower-order DSD moments could improve radar rain rate retrievals. In this paper we use radar attenuation, which is approximately the 1^{st} moment of the DSD, as a constraint to estimate profiles and layer-averaged rain rates below an airborne W-band Doppler radar.

The observations we are using are from the NOAA Physical Science Division (PSD) W-band radar (Moran et al. 2012) deployed on a NOAA P-3D aircraft for 7 flights during the CALWATER2 field program off the US West coast in 2015 (Ralph et al. 2016). This paper presents an analysis of processing measured equivalent radar reflectivity factor profiles to estimate precipitation rate using the observed decrease of Z_{em} with range below the aircraft. The rain rate is approximately proportional to the attenuation coefficient in rain (i.e., the slope of the reflectivity profile, assuming a prevalence of attenuation effects over changes of non-attenuated reflectivity Z_e) as described in Matrosov (2007). A second but related method to estimate rain rate uses the measured normalized radar cross section ($NRCS_m$) retrieved from the return of the ocean surface. Since *NRCS* is fairly well-characterized as a function of wind speed and angle relative to nadir (Li et al. 2005), the calculated $NRCS_c$ is independent of radar attenuation. Thus, the difference between the measured and calculated *NRCS* represents the total column attenuation, which is also known as the path integrated attenuation (PIA). As with the reflectivity gradient rain rate method, the estimated PIA is related to rain rate such that PIA yields an estimate of the total column average rain rate below the aircraft (Meneghini et al. 1983). The total rain rate estimates retrieved from the W-band radar measurements are compared to estimates from two other systems on the P-3: a stepped frequency microwave radiometer (*SFMR*, Uhlhorn et al. 2007) and a wide swath radar altimeter (*WSRA*, Walsh et al. 2014).

2.0 **Experimental Details**

a. CALWATER2

The CalWater-2015 field deployment off the US West coast included NOAA's flagship Research Vessel *Ronald H. Brown (RHB)*, as well as a P-3 and G-IV aircraft. The DOE-sponsored Atmospheric Radiation Measurement (ARM) Cloud Aerosol Precipitation Experiment (ACAPEX) campaign provided the DOE ARM Mobile Facility 2 (AMF2) observing system, mounted on the NOAA vessel, as well as the DOE G-1 aircraft and support for aerosol and microphysics sensors at the coast. The NASA ER-2 aircraft flew several missions as well with remote sensors tailored partly for validation of a prototype space-based sensor being tested on the International Space Station. The California Department of Water Resources (DWR)-sponsored statewide extreme precipitation network, tailored to observe landfalling ARs, was a foundation of the experiment. The observation period was January through March, 2015. Here we discuss measurements taken on the NOAA P-3 aircraft.

b. P-3 measurements

NOAA's WP-3D Orion aircraft are equipped with a unique array of scientific instrumentation, radars and recording systems for both *in situ* and remote sensing measurements of the atmosphere, the earth and its environment (http://www.omao.noaa.gov/learn/aircraft-operations/aircraft/lockheed-wp-3d-orion). Rain rate values were estimated from two systems on the P-3: the SFMR and the WSRA. These estimate rain rate averaged over altitudes below the aircraft. *In situ* sensors provided flight level meteorological and navigation information. The P-3 also deployed 80 dropsonde profilers during the period in the region near 37° N Latitude and 127° W Longitude.

The observations we are focusing on are from the NOAA Physical Science Division (PSD) W-band radar deployed on the P-3 for 7 flights between January 27 and February 9, 2015. The radar is described in depth by (Moran et al. 2012). Initial deployments were ship-based (Moran et al. 2012; Ghate et al. 2014) but aircraft deployments began in 2013 (Fairall et al. 2014). Aircraft deployments include tropical storm Karen, hurricane Patricia, and CALWATER2.

c. *Radar Settings*

The W-band radar operated in one Doppler spectra mode with a focus on measuring rain below the aircraft. Doppler spectra were recorded to disk every 0.3 seconds and the first 3 moments (i.e., 0^{th}, 1^{st}, and 2^{nd}) were calculated to estimate reflectivity, mean Doppler velocity, and mean Doppler velocity spectrum width. Pertinent radar operating parameters are listed in Table 1. Note that the first range gate was set to 489 m below the aircraft to avoid destroying the receiver from strong surface returns when the aircraft was below 500 m altitude.

3. Radar-Precipitation Relationships

a. Processing for Radar Reflectivity and Surface Cross-section

For distributed targets within a radar resolution volume, the measured reflectivity factor, $Z_{em}(r)$ ($mm^6\ m^{-3}$), at range r (km) is related to the received power, $P_r(r)$, via

$$Z_{em}(r) = C_{radar}\frac{\lambda^4}{\pi^5 |K|^2} P_r(r) r^2 \quad (1)$$

where $|K|^2 = 0.82$ is the magnitude squared of the complex refractive index of water at the radar operating wavelength λ=3.17 mm, and C_{radar} is the radar calibration constant that incorporates all radar gains and losses. After calibrating the PSD W-band radar antenna at an antenna range and with careful determination of system losses (including a 1.6 dB radome loss – see section 3c), absolute reflectivity accuracy is expected to be approximately ±1 dB. Due to attenuation at W-band frequencies, the equivalent reflectivity factor, $Z_e(r)$ at range r, is given as

$$Z_e(r) = Z_{em}(r)\exp[0.2\ln(10)\int_0^r \gamma_{total}(s)ds] \quad (2)$$

where γ_{total} is the total specific attenuation (dB km^{-1}) at range s (km) of length ds (km) and is composed of specific attenuations from oxygen γ_o, water vapor γ_{vapor}, cloud γ_{cloud}, and precipitation γ_{rain}. The total specific attenuation can be expressed at

$$\gamma_{total}(s) = \gamma_o(s) + \gamma_{vapor}(s) + \gamma_{cloud}(s) + \gamma_{rain}(s) \quad (3)$$

With regard to surface returns, the W-band radar observes a strong spike in measured reflectivity factor, Z_{em}, from the ocean surface (Fairall et al, 2013) which is referred to as the ocean scattering cross section, $\sigma_0 = \eta_0 * dR$ (where dR is the radar range gate thickness). Measured reflectivity factor is converted to measured normalized radar cross-section ($NRCS_m$) using

$$NRCS_m = 10*\log_{10}(\sigma_0) = 10*\log_{10}[\frac{\pi^5 |K^2|}{\lambda^4} dR] + dBZ_{em} - 180 + Corrections \quad (4)$$

where dBZ_{em} = $10\log_{10}(Z_{em})$, 180 is a conversion factor converting reflectivity factor from mm^6 m^{-3} to m^3 and the corrections include 1.6 dB for the radar window in the belly of the aircraft 2-way attenuation plus combined attenuation along the beam by water vapor, oxygen, rain, and clouds. At W-band and with 25 m range resolution, the first term on the right hand side of (4) is 137.9. The equation to estimate $NRCS_m$ is

$$NRCS_m = dBZ_{em} + 137.9 - 180 + 1.6 + G(h) \tag{5}$$

where *G(h)* is the total path-integrated attenuation (PIA) by water vapor, oxygen, clouds, and rain.

b. Rain Profile Retrievals using Reflectivity Gradient

After correcting for attenuation, the simplest rain rate *R* in mm hr^{-1} retrievals are typically based on Z_e-R power-law relationships of the form

$$Z_e = a_Z R^{b_Z} \tag{6}$$

Z_e-R relationships are estimated in several ways: e.g., fitting observed Z_e versus surface-based rain measurements or using airborne or ground-based measurements of the rain DSD to compute non-attenuated values of Z_e and R. Rain rate can be expressed as a function of Z_e by inverting (6)

$$R = [Z_e / a_Z]^{1/b_Z} = a_Z^{-1/b_Z} Z_e^{1/b_Z} \tag{7}$$

Note that expression (7) is poorly posed for retrieving rain rate at W-band, in part, because Z_e at W-band includes both Rayleigh scattering regime for small raindrops and Mie scattering regime for drops greater than about 0.8 mm in diameter. The Mie scattering regime reduces the value of Z_e as rain rate increases. Dual-polarization methods can alleviate some of these problems and improve rain rate estimates (Bringi and Chandrasekar 2001), but these methods are not applicable at nadir views.

The relationship between rain specific attenuation and rain rate can be expressed with a power-law of the form (Matrosov 2007)

$$\gamma_{rain} = a_{\gamma} R^{b_{\gamma}} \quad (8)$$

Some estimated coefficients from previous studies are given in Table 2. Given a data scatter in the $\gamma_{rain} - R$ correspondence the relation (8) could be assumed to be linear with $b_{\gamma} = 1$ (Matrosov 2007). Thus, a linearized mean relationship between the attenuation coefficient γ_{rain} and rain rate is

$$R = c\gamma_{rain}[\frac{1.1}{\rho_a(z)^{0.45}}] \quad (9)$$

where c=1.11 km/dB mm/h as estimated from T-matrix modeling using drop size distributions (DSDs) collected with the Joss-Waldvogel disdrometer during a Hydrometeorology Test Bed (HMT) field project in California (Matrosov 2010), and the term on the right is a dimensionless correction factor accounting for an increase in rain drop fall velocity as the air density ρ_a (in kg m^{-3}) decreases with height *z*, above the surface. For linear $\gamma_{rain} - R$ relationships, a density correction of 1.04 was used which corresponded to an altitude of 1.0 km and CALWATER2 atmospheric conditions.

Since attenuation coefficients are usually specified in dB/km, they can be related to the vertical gradient of measured dBZ_{em} as

$$\frac{d(dBZ_{em})}{dz} = \frac{d(dBZ_e)}{dz} + 2(\gamma_{rain} + \gamma_v) \quad (10)$$

where the first term in the right hand side describes changes of non-attenuated reflectivity dBZ_e, assuming the cloud attenuation can be neglected compared to rain attenuation, and the factor of 2 in this equation arises because the radar has a two-way path; $\gamma_v = \gamma_o + \gamma_{vapor}$. A stratus cloud with a liquid water content of 0.1 g/m^3 would have an attenuation of approximately 0.4 dB/km – roughly comparable to rain with rate of 0.5 mm/hr (e.g., Matrosov 2009). If the vertical gradient of dBZ_e (non-attenuated reflectivity) is small compared to that due to attenuation, the rain attenuation can be computed from the slope of dBZ_{em} vs altitude

$$\gamma_{rain} = 0.5\frac{d(dBZ_{em})}{dz} - \gamma_v \qquad (11)$$

where each term in (11) is height dependent.

The ‘Bootstrap’ values given in Table 2 are obtained from relationships based on NRCS rain rates and observed attenuation and reflectivity, i.e., solely determined by Calwater2 W-band observations. The P-3 values are computed from a Droplet Measurement Technologies Precipitation Imaging Probe (PIP) which sizes drops in 62 equally-spaced bins from 0.10 to 6.2 mm diameter.

c. Path Integrated Rain Retrievals

The radar backscatter from the sea surface allows another method to compute the path-averaged rain rate from the total attenuation from the aircraft to the surface. For our purposes here we restrict the analysis to nadir pointing profiles only, so at a given wavelength the $NRCS_c$ is a function of wind speed only.

$$NRCS_c = |F(0)|^2 / mss = f(\mathrm{U}_{10}) \qquad (12)$$

where U_{10} is the wind speed at a height 10 m above the ocean, $F(0)^2$=0.32 is the Fresnel reflection coefficient at 20 C for seawater at W-band at normal incidence and *mss* is the mean squared slope of the surface waves. Thus, the difference between the measured $NRCS_m$ and the value, $NRCS_c$, gives a path-integrated attenuation (PIA)

$$PIA_R = NCRS_c - NCRS_m - G_v(h) \tag{13}$$

where G_v is the gaseous attenuation.

$$G_v(h) = 2 * \int_0^h \gamma_v(h) dh \tag{14}$$

Values of γ_v were obtained using the atmospheric absorption methods from the International Telecommunications Union (/www.itu.int/dms_pubrec/itu-r/rec/p/R-REC-P.676-3-199708-S!!PDF-E.pdf). For CALWATER2 we computed G_v =2.2 dB for h=alt=2.5 km using the mean water vapor, temperature and pressure profiles from 19 CALWATER2 sondes dropped in the observation region by the NOAA G-IV on 05 Feb. 2015 (precipitable water path of 2.2 cm from the surface to 2.5 km altitude). Profiles of dBZ_{em} were corrected by 1.6 dB+$G_v(h)$+0.6 dB. The value 1.6 dB is the transmission window loss and 0.6 dB is a correction to force observed NRCS to agree with experimental values in Li et al. (2005) at a wind speed of 1.0 m/s. $G_v(h)$ was 0.07 dB at the first radar range gate and 2.20 dB at the surface.

The NRCS – based rain rate can be computed as

$$R_{nc} = c\, k(z) \frac{NRCS_c - NRCS_m - G_v(h)}{alt} \tag{15}$$

The advantage of (15) is that it does not require near-uniform vertical profiles of rain, but gives mean rain rate between the aircraft and the surface. The disadvantage is that it requires a specification of $NRCS_c$. $NRCS_m$ is computed from Z_{em} at the surface as per (4). The model for $NRCS_c$ we are using is

$$NRCS_c = 14.1 - 0.2 * U_{10} - .004 * U_{10}^2; \quad (16)$$

based on fits to $NRCS_m$ for clear sky data in previous flights (but bias corrected as described above); U_{10} is obtained from the SFMR measurements. The coefficients in (16) correspond to U_{10} in m/s. If (15) yields a negative number, we set it to zero.

d. Profiles of Z_e vs Z_{em}

A considerable amount of work is in the literature concerns retrieving the true (i.e., non-attenuated) Z_e profile from the radar-observed profile. The simplest approach is to combine (10) with a specification of attenuation in terms of Z_e as in (11)

$$\gamma_{rain} = \alpha_\gamma Z_e^{\beta_\gamma} \quad (17)$$

In this case, Iguchi and Meneghini (1994) show that the Hitschfeld and Bordan (1954) relation can be expressed as

$$Z_e(h) = \frac{Z_{em}(h)}{[1 - qS(h)]^{1/\beta_\gamma}} \quad (18)$$

where

$$S(h) = \int_0^h \alpha_\gamma Z_{em}^{\beta_\gamma}(h')dh' \quad (19)$$

and

$$q = 0.2\beta_\gamma \ln(10) \quad (20)$$

Note that the integral *S(h)* is in terms of the <u>measured</u> Z_e, so the right hand side of (18) is solely in terms of measured quantities. For example, if we take the linear attenuation coefficient - rain rate relationship and the bootstrap Z_e-R relationship from Table 2, then, $1/\beta_\gamma = 1.0$, $\alpha_\gamma = 0.035$ and q=0.46.

The integral given by (19) is related to the attenuation. Using (18) we can compute an integral estimation of attenuation

$$\gamma_{\text{int}} = -\frac{1}{qh}\ln[1 - qS(h)] \tag{21}$$

From which we can calculate a layer-averaged profile of rain rate at each timestep. If we set *h* to the altitude of the aircraft, then (21) yields an average attenuation coefficient which can be used to estimate rain rate similar to the NRCS approach. The advantage of using (21) is that it does not require that vertical changes in unattenuated Z_e are small compared to reflectivity changes due to attenuation (as the gradient methods require).

4.0 Processing and Analysis

Only two flights (Feb 05 hrs 19, 20, 21; and Feb 06 hr 19) yielded significant 'stratiform' rain that is suitable for our analysis. Here we use the term stratiform to describe wide-scale, weakly convective precipitation associated with mid-latitude AR's. We are not using it in the usual radar jargon referring to broad areas of precipitation in outflow regions from deep tropical convection. The flight on Feb 07 had significant rainfall which is suitable for applying the NRCS approach but too patchy to be able to claim relative vertical homogeneity (i.e., the presence of uniform rain everywhere in a layer from the aircraft altitude to the surface). On Feb. 05 the aircraft was flying below a large region of precipitating clouds (i.e., it was not in cloud).

In some periods there were low-level 'scud' clouds below the aircraft with tops around 0.5 km. Radar measurements from the NOAA ship *Ronald H. Brown* indicated cloud tops at 7 km altitude with a freezing level bright band at about 3 km altitude.

An example of a radar profile measurements is shown in Fig. 1. The P-3 location during the flight is shown in Fig. 2 with indications of 10-m wind speed from the SFMR in Fig. 2a and a visible satellite image in Fig. 2b. Measured and parameterized values of NRCS are shown in Fig. 3a with resultant rain rate in Fig. 3b. In Fig. 4 we show rain rate estimates from the SFMR and the WSRA for the entire 3-hr period. The WSRA has been biased corrected for slow variations in the transmit power. Some elements were not operating correctly and the problem was intermittent. The comparison between NRCS and SFMR retrievals is better but still not good for lighter rain rates. At rain rates greater than about 2 mm/hr the agreement is better. The correlation coefficient between NRCS and SFMR rain rates is 0.71 while for NRCS - WSRA rain rates it is 0.60.

The peak NRCS rain rate in Fig. 4 is about 10 mm/hr which is the approximate limit of the radar when flying at 2.5 km with 20 m/s 10-m wind speed. This is because the surface return is no longer detectable for greater rain rates (e.g., see gap in the surface return line at 19 hrs 20 min UTC in Fig. 1).

a. Processing Methods

We have examined several methods to estimate rain rate for the measured reflectivity profiles from two points of view: 1) time series of layer-averaged rain rate computed from each profile of Z_{em} and 2) profiles of radar variables averaged in bins of rain rate. The time series methods are:

1) Compute a linear regression for each observation of dBZ_e vs h of the form

$$dBZ_{em} = dBZ_{emi} + slope * h$$

where the slope of the regressions is $slope = \frac{d(dBZ_{em})}{dh} = -\frac{d(dBZ_{em})}{dz}$.

Rain rate is then estimated from this slope using (9) after accounting for the gaseous attenuation. The intercept, dBZ_{emi}, is reflectivity at the aircraft height (h=0) which is an estimate of the unattenuated dBZ_e (valid when rain is observed in the first range gate and assumes that rain is present in the whole layer from the aircraft altitude to the surface).

2) Compute a layer-averaged attenuation as a ratio= $(dBZ_{em}(i)\text{-}dBZ_{em}(j))/(alt(i)\text{-}alt(j))$ and get an estimate of rain rate from the ratio using (9). This estimate is somewhat akin to the *NRCS* estimate but does not depend on a surface backscatter model. Here we have used range gates at altitudes of 1.83 and 0.20 km.

3) Compute the integral of parameterized attenuation via (19) and estimate layer-averaged attenuation/rain rate via (21).

The bin-averaged methods use rain rate from the NRCS method:

4) Average the reflectivity, $\langle dBZ_{em}\rangle$, profiles in bins of rain rate; the mean attenuation profile for that bin is $d(\langle dBZ_{em}\rangle)/dh$. Thus, it yields *profiles* of mean attenuation (and therefore rain rate) for the average sample.

5) Average profiles of the derivative of the dBZ_{em} in bins of rain rate, $\langle d(dBZ_e)/dh\rangle$.

Note that the surface reference (i.e., NRCS) and reflectivity gradient approaches have been used with the spaceborne W-band radar aboard CloudSat.

b. Rain rate Time Series

An important issue to solve is how to treat the non-ideal nature of the non-attenuated reflectivity profiles in the processing (Matrosov 2009). Examples of three types of dBZ_e profiles are shown in Fig. 5. A glance at Fig. 1 shows periods when there is no rain at aircraft flight level or the first observable range gate (e.g., the period from 19 hrs 5 min to 13 min UTC). Thus, a vertical derivative will indicate negative attenuation near the first range that has precipitation (see the red profile in Fig. 5). Other periods (e.g., 19 hrs 55 min to 60 min) have no return in the entire profile – that is, zero rain rate. The blue line in Fig. 5 shows a profile where rain only occupies the height region above 1 km. The black line in Fig. 5 shows a case with significant return throughout the profile; there is a hint of sea spray causing an increase below 200 m.

c. Time Series

We have examined rain rate estimates using methods 1 and 2. These are pure rain dBZ_e gradient based approaches. Both methods can produce negative rain rates and substantial overestimates of the rain rate when the precipitation below the aircraft is inhomogeneous (i.e., rain is present not everywhere below the aircraft). One simple check to avoid the worse cases is to require the gradient be positive or to require that the dBZ_{em} at the first usable range gate has measurable rain and that the dBZ_{em} at that range gate exceeds the value of dBZ_{em} near the surface. For example, we require $dBZ_{em}(i)>0$ and $dBZ_{em}(i)-dBZ_{em}(j)>-5$ dB (not zero because the lower range gates have higher noise levels – green line if Fig. 5). For values that do not meet the criteria, we set the rain rate =0. Fig. 6 shows the rain rate time series with methods 1 and 2 as defined earlier and the NCRS-based method. The three methods give roughly similar results when the rain is reasonably homogeneous although the gradient methods are noisier. Note overestimates with the gradient methods at the edges of rain sections for which rain is present at all altitudes and recall the NRCS method does not rely on rain being present at all altitudes.

Another issue is the consistency of the NRCS – based rain rate and the dBZ_e and attenuation relationships (Eqs. 6 and 8). Shown in Fig. 7a is the intercept of the linear fit of dBZ_{em} with range versus NRCS rain rate; the intercept occurs at h=0 so it is unaffected by attenuation. Fig. 7b shows a scatterplot of attenuation coefficient as determined by the slope of the dBZ_{em} profile at every time step versus rain rate. Fig. 8 is a plot of the attenuation vs the dBZ_{em} intercept; this relationship is used in the attenuation correction for the dBZ_{em} profile (Eq. 18). Note that for reflectivities greater than about 60 mm^6m^{-3} (~17.8 dBZ), the derived power-law fit between attenuation coefficient and reflectivity is generally not appropriate. This may be a consequence of non-Rayleigh backscatter at W-band, unmeasured absorption between the aircraft and the first range gate, or the effects of wetting of the radar window when flying in heavy rain.

d. Bin-averaged Profiles

Fig. 9 shows profiles of dBZ_{em} and vertical Doppler velocity w averaged in bins of rain rate as determined by the NRCS method for the three hour period on Feb. 5. The bin edges for these results are rain rate = [0, 0.25, 0.7, 1.5, 3, 6, 13] mm/hr; all rain rate averages in the remainder this paper use these edge limits. The SFMR- and WSRA-based rain rates were too noisy and uncertain to use as an index for bin averaging. The measured Doppler vertical velocity is corrected for the pitch component of aircraft motion relative to the air via

$$w_c = w_m + \sin(pitch)[-SOG*\cos(\psi - COG) + U_w*\cos(\psi - Dir)] \qquad (22)$$

The residual given by (22) should be the mean gravitational velocity of the precipitation. Here *SOG* is the aircraft speed over ground (between 100 and 140 m/s), COG is the aircraft course over ground, *pitch* is the aircraft pitch angle, ψ aircraft heading, U_w and *Dir* are the wind speed (taken from the SFMR) and wind direction (taken from the P-3 flight level data). Eq. 22 is derived from the corrections in Fairall et al. (2013) when aircraft roll=0. Some factors to note in Fig. 9:

1) The mean reflectivity value near the surface for the maximum rain rate is -16 dBZ which is greater than, but close to, the radar noise level (-24 dBZ see Fig. 5).
2) The slopes at lower rain rates are confined to the upper part of the profile and are actually larger than the slopes for intermediate rain rates. This likely indicates inhomogeneous profiles with most of the rain confined within 1 km below the aircraft. Thus, attenuation deduced from this regime is not reliable (i.e., gradients of non-attenuated reflectivities are not small compared to the gradients due to attenuation). The increase in fall velocity as the drops approach the surface suggests evaporation, which preferentially removes smaller drops.
3) The dBZ_{em} values at the top of the measured profiles for the two largest rain rate bins are about the same. The slope for the highest rain rate shows much more attenuation so a lot of the signal has been lost between the aircraft and the first range gate (about 10 dB).
4) Fall velocities are between 1 and 3 m/s and roughly increase with rain rate. These correspond to fall velocities for 0.2-0.4 mm diameter droplets which are typical for light rain. The W-band radar is less sensitive (relative to the Rayleigh scattering regime) to droplets larger than about 1 mm. Thus, smaller drops with lower fall velocities are more heavily weighted than for radars at longer wavelengths (e.g., K_a-band).

Finally, we present attenuation profile and rain rate profiles obtained by averaging the profile of the vertical derivative of dBZ_{em} in rain rate bins (method 5). While individual 0.3 s dBZ_{em}

profiles yield a noisy derivative profile, when averaged the results are reasonably smooth (see Fig. 10a). We then use (9) and (11) to compute profiles of rain rate (Fig. 10b). In the latter case we have multiplied the rain rate by the fraction of bins with detectable rain to yield an actual rain rate including the dry periods.

e. Attenuation Corrections of Observed Reflectivity

In order to apply (18) to correct the measured dBZ_{em} for attenuation we must integrate along the entire propagation path from the aircraft to the surface. However, the radar's first range gate is 0.5 km below the aircraft. Thus, we need to fill in the dBZ_{em} profile from the aircraft out to the first range gate. We have done this by fitting a linear regression to the mean dBZ_{em} profile starting at range gate 6 and ending at range gate 25. Then, using the slope and intercept of the fit to the profile, we extrapolate dBZ_{em} values in 19 additional range gates between range gate 1 and the aircraft altitude. This is a total of 169 range gates going from the surface to the aircraft altitude. This is illustrated in Fig. 11 where rain rate bin-averaged profiles of mean dBZ_{em} are shown for 6 selected rain rate bin mean values. The extrapolated portion of the profiles are shown as dotted symbols. Two versions are shown: 1) the mean dBZ_{em} when rain is present and the threshold conditions (SNR>-10 dB and reflectivity at the 5^{th} range gate is – 5 dB greater than the near-surface atmospheric reflectivity) are met and 2) a mean that is the average normalized by the number of profiles that pass the criterion divided by the total number of profiles. The normalization affects the values of dBZ_{em} but not the slope. For the lowest rain rate bin 27% of the profiles meet the threshold criterion; for the highest bin 100% do so.

We have used the average measured dBZ_{em} profiles in rain rate bins and applied (18) to yield 'true' dBZ_e (i.e., with attenuation removed). We experimented with different versions of the γ-Z_e given in (17); α_γ=0.050, β_γ=1.0 and α_γ=0.026, β_γ=1.1. The first set of coefficients produced larger corrections to the lower part of the profile for the cases with greater rain rates. If we increase from α_γ=0.026 to α_γ=0.055, then the results are similar. The main thing to notice from Fig. 12 is that the corrected profiles are not vertically homogeneous. The most inhomogeneous is the profile for the highest rain rate bin (average 7.8 mm/hr). In principle, we might remove some of the vertical gradient by adjusting the coefficients. It turns out this quickly leads to a singularity because $qS(h) > 1.0$. For example, this occurs for the higher rain rates profile if we increase α_γ=0.050 to α_γ=0.055. It is clear that, given uncertainties in the form and coefficients of (18) and extrapolation between the aircraft and the first range gate, that there is a practical limit on the total dBZ_e correction that can be made. For example, a 20 dB correction would require $1 - qS(h) = 0.01$, which is likely beyond the accuracy limit. Iguchi and Meneghini (1994) provide an alternative to (18) where dBZ_e is known at the end of the path. Thus we could explore using *NRCSm/NRCS* to fix the bottom of the corrections.

Fig. 13 shows a layer-averaged rain rate using (21) and (9) where h=2.3 km. This approach gives a smoother representation than methods 1 and 2. However, it suffers from the same ambiguity problem as the profile retrieval method when $q*S$ approaches 1.0.

f. Summary Rain rate Statistics

In Table 3 we compare simple statistics for the different rain rate estimates. We have added one estimate that is independent of the W-band radar, Rain2 – the mean of WSRA and SFMR rain rates. Rain2 has the same mean rain rate as rain from NRCS. The grand mean rain rate across all methods is 1.12 ±0.16 mm/hr; the mean while raining is 2.26 ±0.27 mm/hr. Note the correlation with the NRCS rain rate is lower while raining for methods 1 and 2 and the integral method. This is because the excursions from zero to finite numbers between non-rainy and rainy periods add correlation for those methods. When the zero periods are eliminated, the correlation decreases.

5.0 Discussion and Conclusions

In this paper we examined several approaches to estimating rain rate time series, profiles, and statistics using the radar reflectivity. The data are from the PSD W-band Doppler radar deployed on a NOAA P-3 aircraft during the CALWATER2 field program. Our primary goal was to investigate the use of the radar signal attenuation to estimate rain rate below the aircraft (observation altitude was 2.5 km). The analysis is limited to three hours from a flight in wide-scale frontal precipitation on Feb. 5, 2015. In principle, profiles of rain rate can be computed from the profile of attenuation. However, individual profiles (3 Hz acquisition rate) may be poorly sampled because of the patchy nature of precipitation – this leads to noisy vertical derivatives.

The relationship of attenuation coefficient to the rain rate was found to be near-linear and quite robust with good comparisons of our observations with several others in the literature. At rain rates near 1 mm/hr and below the observed attenuation coefficient levels off - a possible consequence of cloud attenuation. The relationships of reflectivity factor with rain rate or attenuation coefficient were less robust. Our W-band radar measurements were not a good fit to an assumed power law of $\gamma = \alpha_\gamma Z_e^{\beta_\gamma}$ (Fig. 8). This was not an issue with the fits to computations using DSD's. Z_e-R relationships are rather flat because due to Non-Rayleigh scattering effects at W-band reflectivity is weakly dependent on the larger rain drops. The significance is not obvious because the results are somewhat sensitive to the criteria or thresholding used to determine the slopes.

The NRCS method provided the most consistent estimate of layer-averaged rain rate from the W-band. It is superior to Rain2, which is the average of rain rates derived from the SFMR and WSRA. However, WSRA based estimates might be superior if the instrument was operating optimally. The three other methods (1, 2, 3) of estimating layer-averaged rainfall from W-band dBZ_{em} profiles/gradients were not as effective as the NRCS method. The gradient methods were unreliable in inhomogeneous rain distributions when rain is not present at all altitudes below the aricraft; the integral method had problems in the higher rain rates where it was very sensitive to choice of coefficients in the $\gamma - Z_e$ relationship when $qS(h) \cong 1.0$.

Compositing dBZ_{em}, Doppler velocity, or $\frac{\partial dBZ_{em}}{\partial z}$ in bins of rain rate (Figs. 9 and 10a) yields very clean profiles. The lower raintrates have anomalous gradients of dBZ_e in the upper heights, presumably because light rain is occurring at higher altitudes but is not reaching the surface. The profiles of mean gradient-derived rain rate in bins of NRCS rain rate (Fig. 10b) are smooth and the values are consistent (but about 10% higher than NRCS-based rain rate estimates). The use of the Iguchi and Meneghini (1994) method to reconstruct un-attenuated profiles of dBZ_e from the composited observed (attenuated values) was not very robust. The corrections tend to be small for the lower rain rates and subject to singularities for the higher rain rates, for reasons explained by Iguchi and Meneghini (1994). There are more sophisticated methods to deal with this, but, in general, reconstruction methods at W-band remain problematical.

Acknowledgments. The authors wish to thank the NOAA Aircraft Operations - Office of Marine and Aviation Operations flight crew and support team for the making the airborne W-band flights possible. We also thank Marty Ralph, Ryan Spackman, and the rest of the

CALWATER science team. Sergey Matrosov was funded in part by the NASA project NNX16AQ36G.

Data Availability. Raw and processed data for the PSD observations can be found at ftp://ftp1.esrl.noaa.gov/psd3/cruises/CALWATER_2015/ . Dropsonde profiles as Matlab *.mat* files from the G-IV are at ftp://ftp1.esrl.noaa.gov/psd3/cruises/CALWATER_2015/G4/data/. Wband radar data are at ftp://ftp1.esrl.noaa.gov/psd3/cruises/CALWATER_2015/P3/Wband/ with the moment files in netcdf format in the *mom* directory and the P-3 navigation and flight level data in *.txt* files (which includes the SFMR) are in the *Aircraft* directory.

REFERENCES

Bringi, V. N., and V. Chandrasekar, 2001: *Polarimetric Doppler Weather Radar: Principles and Applications*. Cambridge University Press, 664 pp.

Fairall, C.W., S. Pezoa, K. Moran, and D.Wolfe, 2014: An observation of sea spray microphysics by airborne Doppler radar. *Geophys. Res. Lett.*, **41**, doi: 10.1002/2014GL060062.

Frisch, A.S., C.W. Fairall, and J.B. Snider, 1995: Measurement of stratus cloud and drizzle parameters in ASTEX with a K_a -band Doppler radar and a microwave radiometer. *J. Atmos. Sci.*, **52**, 2788-2799.

Frisch, A. S., G. Feingold, C. W. Fairall, T. Uttal, and J. B. Snider, 1998: On cloud radar and microwave radiometer measurements of stratus cloud liquid water profiles. *J. Geophys. Res.*, **103**, 23195-23197.

Ghate, Virendra P., Bruce A. Albrecht, Mark A. Miller, Alan Brewer, and Christopher W. Fairall, 2014: Turbulence and radiation in stratocumulus topped marine boundary layers: A case study from VOCALS-Rex. *J. Appl. Met. Clim*., **53**, 117–135. doi: http://dx.doi.org/10.1175/JAMC-D-12-0225.1.

Haynes, J.M., and 6 coauthors, 2009: Rainfall retrieval over the ocean with spaceborne W–band radar. *J. Geophys. Res*., **114**, D00A22, doi: 10.1029/2008JD009973.

Galloway, J., A. Pazmany, J. Mead, R. E. McIntosh, D. Leon, J. French, S. Haimov, R. Kelly, and G. Vali, 1999: Coincident *in situ* and W-Band radar measurements of drop size distribution in a marine stratus cloud and drizzle. *J. Atmos. Oceanic Tech*., **16**, 504-517.

Hitschfeld, W., and J. Bordan, 1954: Errors inherent in the radar measurement of rainfall at attenuating wavelengths. *J. Meteor.*, **11**, 58-67.

Iguchi, Toshio, and R. Meneghini, 1994: Intercomparison of single-frequency methods for retrieving a vertical rain profile from airborne or spaceborne radar data. *J. Atmos. Oceanic Tech.*, **11**, 1507-1516.

Kollias, P., B. A. Albrecht, and F. D. Marks Jr., 2003: Cloud radar observations of vertical drafts and microphysics in convective rain. *J. Geophys. Res.*, **108**, 4053, doi:10.1029/2001JD002033.

Kollias, P., and 7 coauthors, 2007: The Atmospheric Radiation Measurement Program cloud profiling radars: Second-generation sampling strategies, processing, and cloud data products. *J. Atmos. Oceanic Tech.*, **24**, 1199-1214.

Koschmeider, H., 1934: Methods and results of definite rain measurements. *Mon. Weather Rev.*, **62**, 5-7.

Lee, GyuWon, and Isztar Zawadski, 2006: Radar calibration by gage, disdrometer, and polarimetry: Theoretical limit caused by the variability of drop size distribution and application to fast scanning operational radar data. *J. Hydrol.*, **328**, 83-97.

Lhermitte, R.M., 2002: *Centimeter and Millimeter Wavelength Radars in Meteorology*. Lhermitte Publications, 4040 Lyber Ave, Miami, FL, 500 pp.

Li, Lihua, G.M. Heymsfield, L. Tian, and P.E. Racette, 2005: Measurements of ocean surface backscattering using an airborne 94-GHz cloud radar – implications for calibration of airborne and spaceborne W-Band radars. *J. Atmos. Oceanic Tech.*, **22**, 1033-1045.

Matrosov, S. Y, 2007: Potential for attenuation-based estimations of rainfall from CloudSat. *Geophys. Res. Lett.*, **34**, L05817, DOI:10.1029/2006GL029161.

Matrosov, S. Y., 2009: A method to estimate vertically integrated amounts of cloud ice and liquid and mean rain rate in stratiform precipitation from radar and auxiliary data. *J. App. Met. Clim.*, **48**, 1398-1410; DOI:10.1175/2009JAMC2106.1

Matrosov, S.Y., 2010: Evaluating polarimetric X-band radar rainfall estimators during HMT. *J. Atmos. Oceanic Tech.*, **27**, 122-134.

Meneghini, R., J. Eckerman, and D. Atlas, 1983: Determination of rain rate from a space-borne radar using measurements of total attenuation. *IEEE Trans. Geosci. Remote Sens.*, **21**, 34-43.

Moran, K., S. Pezoa, C.W. Fairall, C. Williams, T. Ayers, A. Brewer, S.P. de Szoeke, V. Ghate 2012: A motion-stabilized W-band radar for shipboard observations of marine boundary-layer cloud., *Bound.-Layer Meteorol*., **141**, 3-24, DOI 10.1007/c10546-011-9674-5.

Ralph, F. M., K. A. Prather, D. Cayan, J.R. Spackman, P. DeMott, M. Dettinger, C. Fairall, R. Leung, D. Rosenfeld, S. Rutledge, D. Waliser, A. B. White, J. Cordeira, A. Martin, J. Helly, and J. Intrieri, 2016: CalWater field studies designed to quantify the roles of atmospheric rivers and aerosols in modulating U.S. West Coast precipitation in a changing climate. *Bull. Am. Meteor. Soc.*, **97**, DOI: http://dx.doi.org/10.1175/BAMS-D-14-00043.1.

Steiner, M. J. A. Smith, and R. Uijlenhoet, 2004: A microphysical interpretation of radar reflectivity – rain rate relationships. *J. Atmos. Sci.*, **61**, 1114-1131.

Tridon, Frédéric, Alessandro Battaglia, and Pavlos Kollias, 2013: Disentangling Mie and attenuation effects in rain using a K_a-W dual-wavelength Doppler spectral ratio technique. *Geophys. Res. Lett.*, **40**, 5548–5552, doi:10.1002/2013GL057454.

Uhlhorn, E.W., P.G. Black, J.L. Franklin, M. Goodberlet, J. Carswell, and A.S. Goldstein, 2007: Hurricane surface wind measurements from an operational stepped frequency microwave radiometer. *Mon. Wea. Rev.*, **135**, 3070–3085, doi: http://dx.doi.org/10.1175/MWR3454.1.

Walsh, E.J., I. PopStefanija, S. Matrosov, J. Zhang, E. Uhlhorn, and B. Klotz, 2014: Airborne rain-rate measurement with a Wide-Swath-Radar altimeter. *J. Atmos. Oceanic Tech.*, **31**, 860-875, DOI: 10.1175/JTECH-D-13-00111.1.

Williams, Christopher R., 2016: Reflectivity and liquid water content vertical decomposition diagrams to diagnose vertical evolution of raindrop size distributions. *J. Atmos. Oceanic Tech*., **33**, 579-595.

Table 1. Specifications of the PSD W-band radar for CALWATER2 flights.

Parameter	**Value**
Radar operating frequency	94.56 MHz
Radar operating wavelength	3.17 mm
Number of range gates	150
Range resolution	25 m
Distance to first range gate	489 m
Distance to last range gate	4214 m
Number of Doppler velocity bins	128
Doppler velocity bin resolution	0.12 m s^{-1}
Nyquist Velocity	7.68 m s^{-1}
Number of spectral averages	9
Minimum detectable SNR	-20 dB
Minimum detectable reflectivity at 1 km	-34 dBZ
Dwell time per average spectrum	0.3 s
Antenna diameter	0.305 m
Antenna gain	46 dB
Antenna beamwidth	0.7 degrees

Table 2. Coefficients for rain rate dependence of Z_e (6) and γ_{rain} (8) at W-band. ‘Bootstrap’ refers to relationship based on NRCS rain rates and observed attenuation and reflectivity. Llhermite and Kollias values are computed from Marshall-Palmer DSD. Matrosov (2007, 2010) values are computed from disdrometer DSD measurements. P-3 PIP calculations are from the airborne *in situ* DSD measurements on 6 February 2015. *Implies γ-Z_e coefficients computed from the Z_e-R and γ-R relationships.

Source	$\mathbf{a_z}$	$\mathbf{b_z}$	$\mathbf{a_\gamma}$	$\mathbf{b_\gamma}$	α_γ	β_γ
Lhermitte (2002)	63	0.67	1.25	0.75	0.0121*	1.12*
Kollias et al. (2003)			0.89	0.83		
Matrosov (2007)			0.81	1.00		
Matrosov (2010) Direct γ-Z_e fit Linear γ-R fit	**36**	**1.03**	1.13 **0.9**	0.89 **1.00**	0.051* **0.033** 0.028*	0.86* **0.97** 0.97*
Bootstrap Direct γ-Z_e fit (Fig.8)	**25**	**0.91**	**0.93**	**1.00**	0.026* **0.035**	1.10* **1.0**
P-3 PIP Direct γ-Z_e fit linear γ-Z_e fit	**23**	**0.94**	**0.70**	**1.00**	0.026* **0.058** 0.040	1.05* **0.85** 1.00
Average Bold **Uncertainty**	28 ±5	0.96 ±0.04	0.84 ±0.09	1.0	0.042 ±0.01	0.94 ±0.06

Table 3. Comparison of mean rain rate (mm/hr) and correlation coefficients for the different methods. The mean while raining is computed by eliminating non-raining periods from the average.

Method	NRCS	Meth. 1 Slope	Meth. 2 ΔZ_{em}	Meth. 3 Integral	WSRA	SFMR
Mean rain rate	1.04	0.98	1.3	1.1	1.7	0.6
Mean while raining	2.1	2.4	3.2	2.5	2.0	1.4
Correlation with NRCS	1.0	0.50	0.58	0.62	0.60	0.71
Correlation NRCS R>0.5 mm/hr	1.0	0.36	0.35	0.47	0.65	0.73
Correlation with Rain2	0.72	0.46	0.45	0.35	0.94	0.96

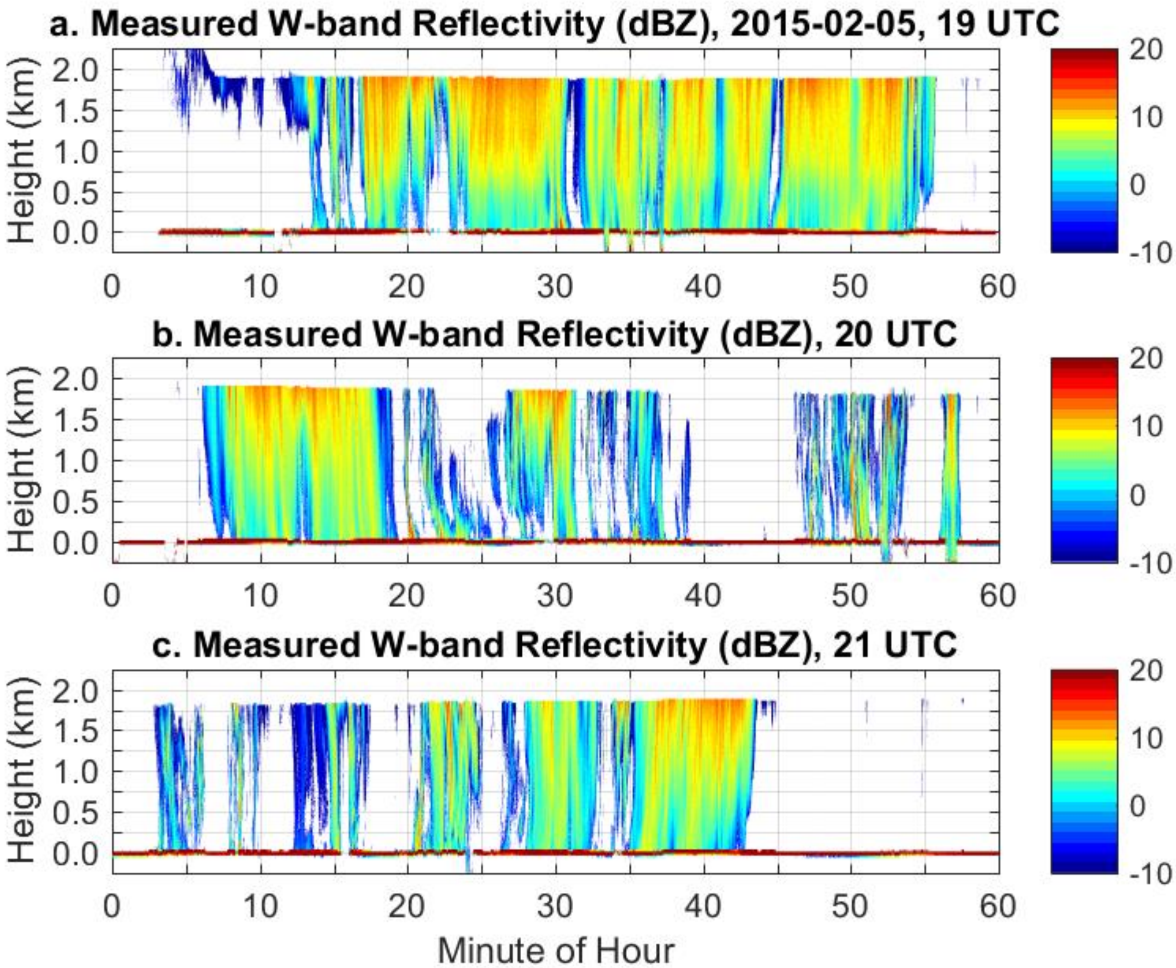

Figure 1. Time-range cross-section of reflectivity (*dBZ_{em}*) for hours 19, 20, and 21 on Feb 05. The vertical ordinate is height above the surface (altitude); the horizontal ordinate is minutes for each hour (UTC) on Feb 05. The surface return is apparent as the bright red line at altitude near 0. The aircraft descended from 5 km to 2.5 km in the beginning of the record. Banking maneuvers are visible as the short periods of extended range in the surface return (e.g., 20 hr 53 min). Note the period just after 19 hr 20 min where attenuation is so great there is no surface return.

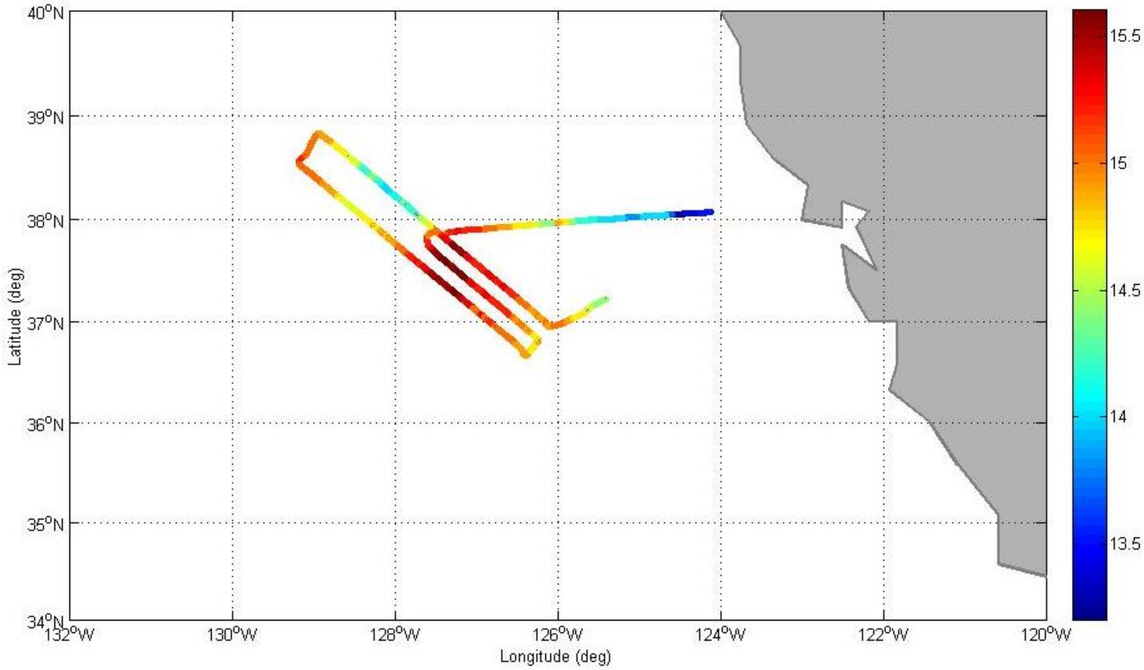

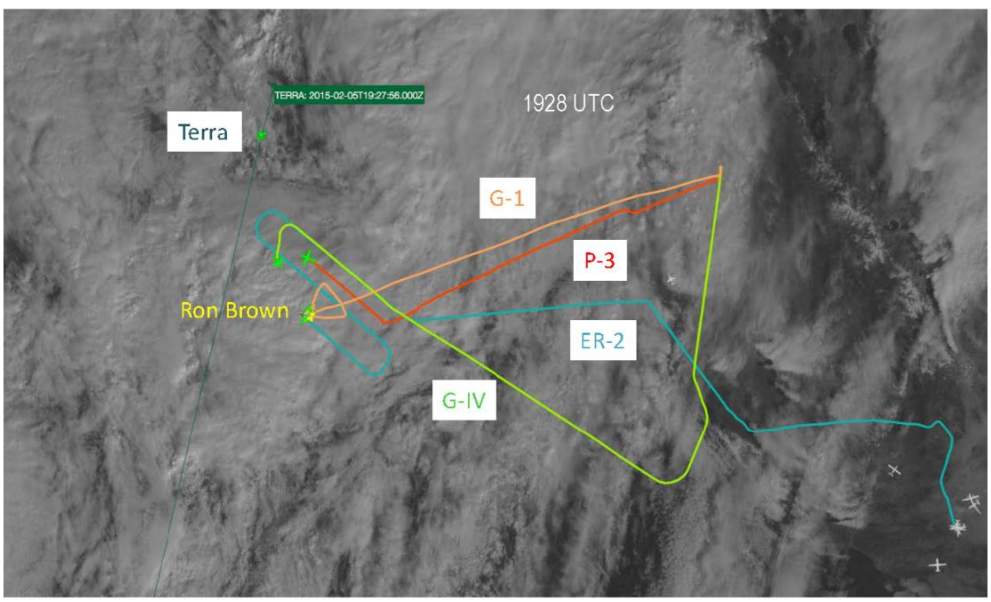

Figure 2. Upper: Flight path of the NOAA P-3 for hours 19-22 Feb 05. The color of the path denotes 10-m wind speed (m/s) from the SFMR. Lower: Satellite visible image with tracks from four aircraft up to 1928 UTC on Feb. 5.

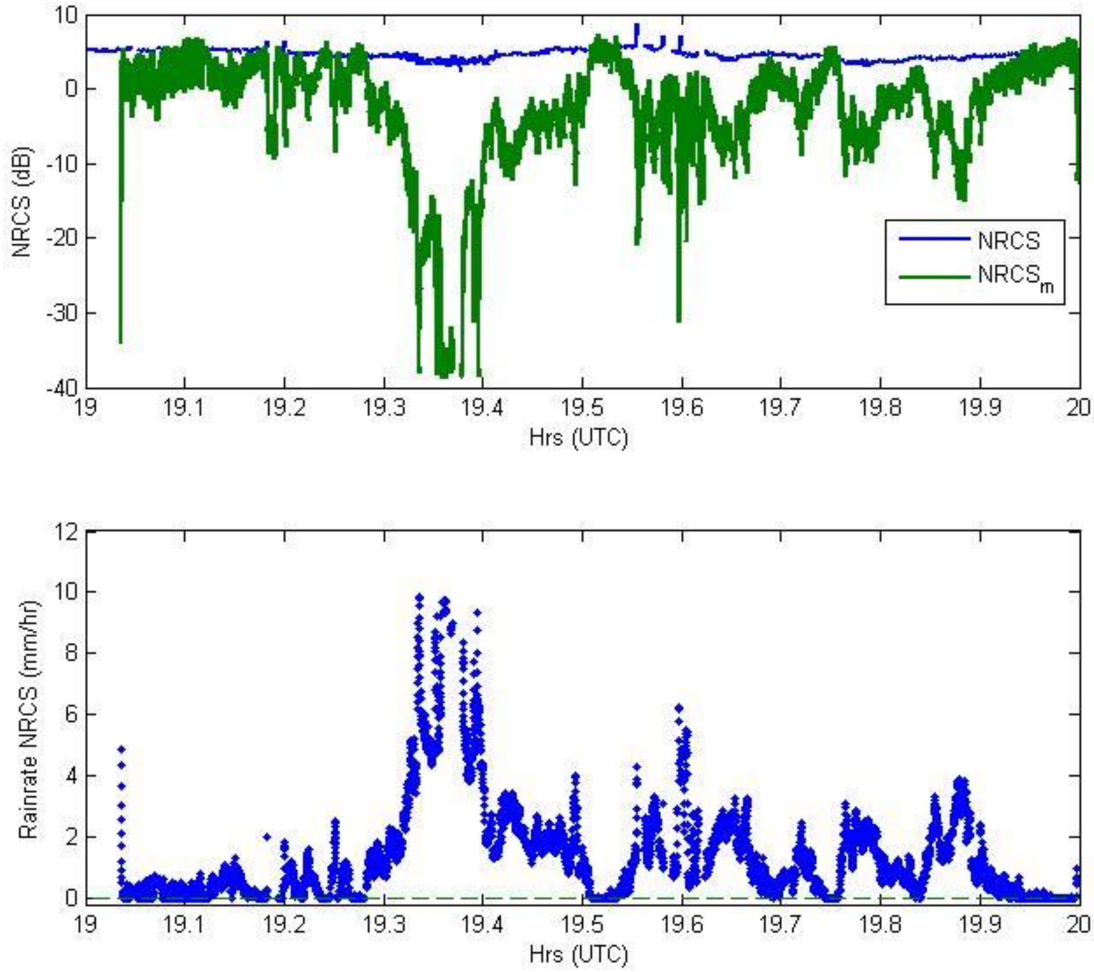

Figure 3. Upper panel: Sample time series of modeled $NRCS_c$ (blue) and $NRCS_m$ measured including attenuation (green) from Feb 05 Hr 19 in CALWATER2. Note a few missing values just after 19.35 where rain attenuation was sufficient to eliminate the surface return (you can see this as a notch in dBZ_{em} in Fig. 1 where the surface return disappears). At the end of the record there is no precipitation so the blue and green lines coincide. Lower panel: precipitation from $NRCS_c$-$NRCS_m$.

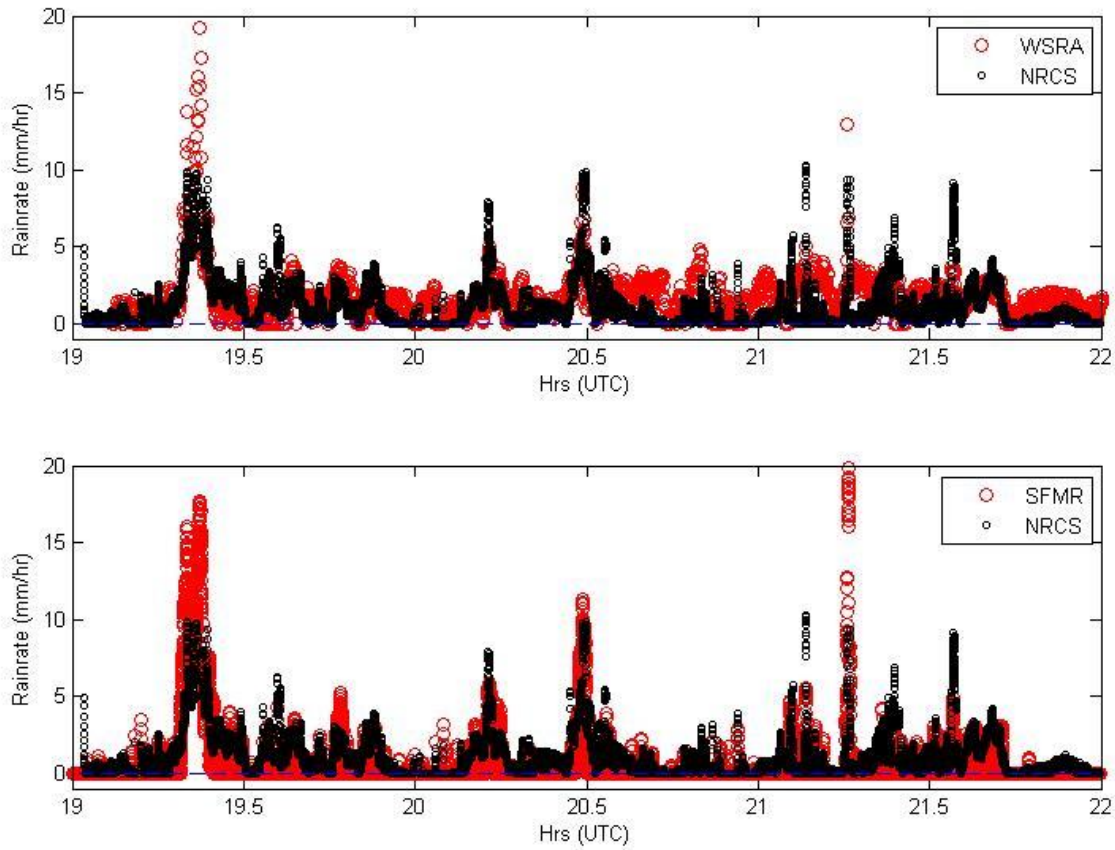

Figure 4. As in Fig. 3. Except a smoothed form of the NRCS rain rate is shown for the entire period 1900 through 2200. The NRCS rain rate is in black, rain rate from the WSRA (upper panel) and SFMR (lower panel) are in red.

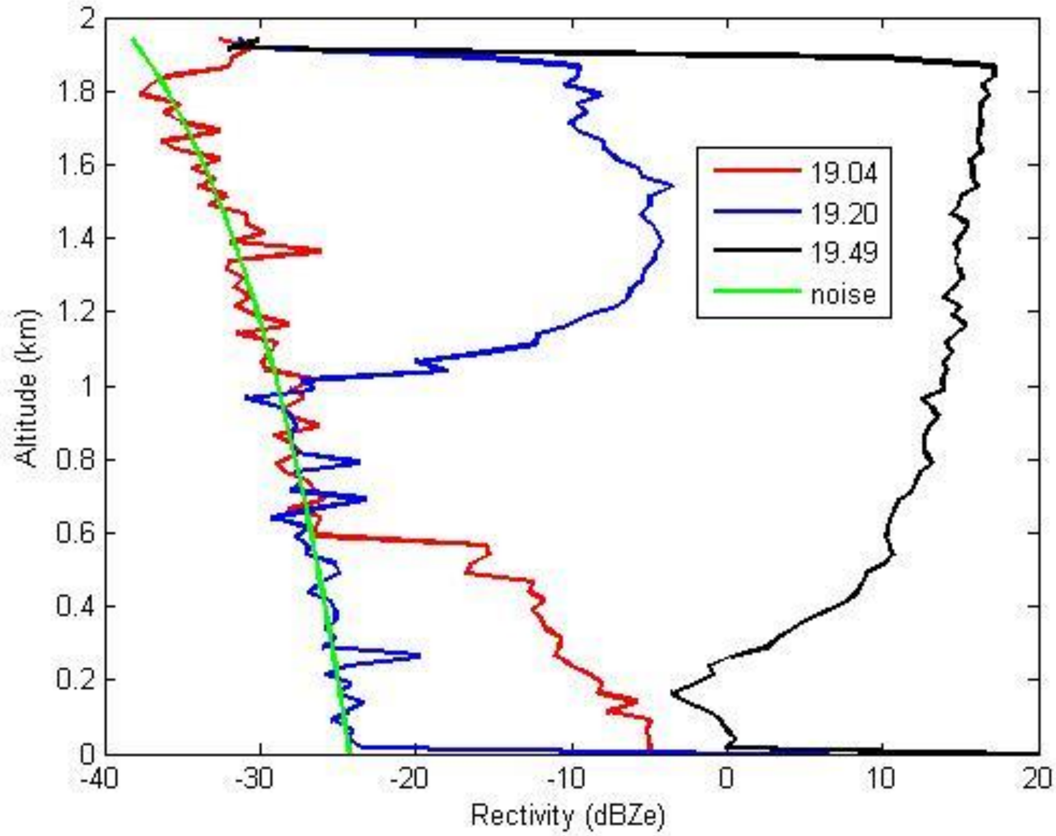

Figure 5. Sample observed reflectivity profiles from hr 19 on Feb. 05. The green line indicates the noise level of the radar (in dBZ_{em} terms it increases with range from the radar). The red line is early in the record with light precipitation from the surface up to 0.6 km. The blue line is later with no precipitation below 1 km. The black line is later still with precipitation all the way to the surface. The legend shows the time within the hour.

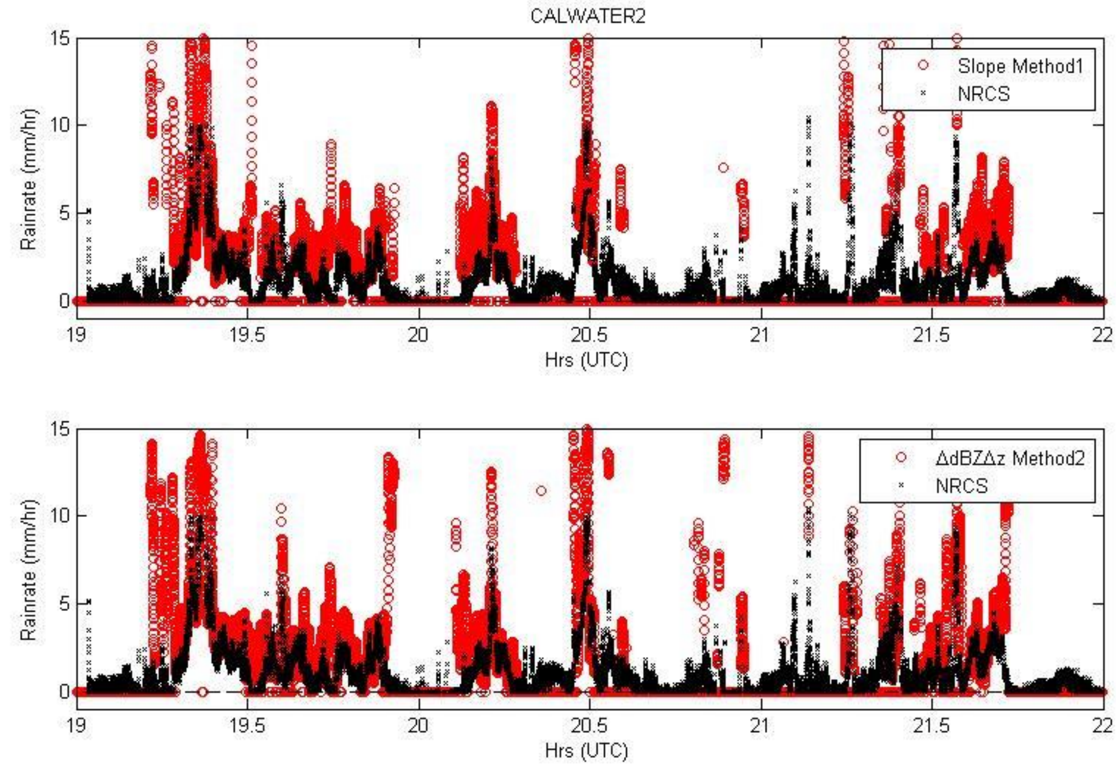

Figure 6. Layer mean radar-derived rain rate estimates from Feb. 05, 2016. The *NRCS* values (black) are compared to two different dBZ_{em} gradient estimates: upper panel, slope method; lower panel, 2-gate differnce method. For method 2 the difference in reflectivity is computed between the two range gates at 1.83 and 0.20 km altitude.

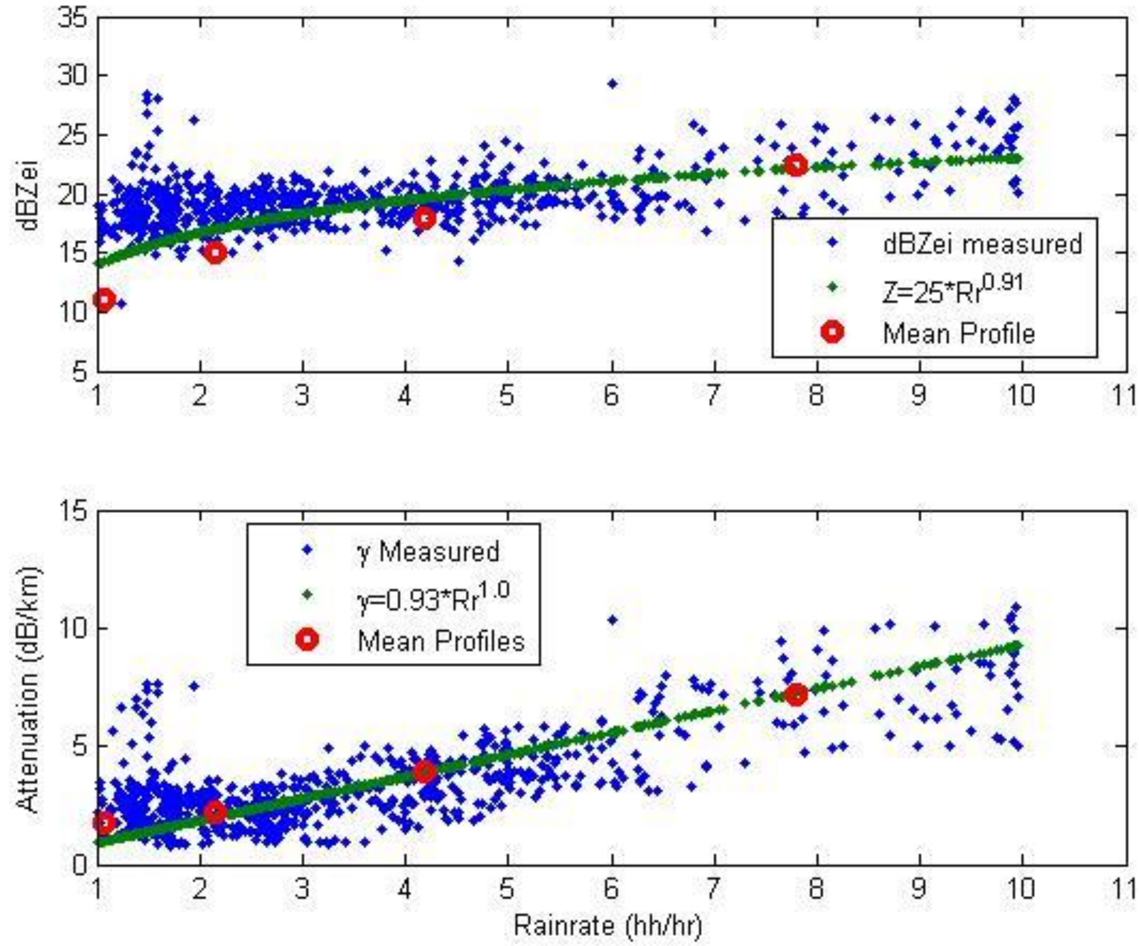

Figure 7. Results from analysis of each profile using regression fits of the form $dBZ_{em} = dBZ_{emi} + slope * h$. Upper panel: W-band dBZ_{em} extrapolated to the aircraft altitude as a function of NRCS rain rate. Lower panel: one-way attenuation coeffcient in dB/km vs rain rate. Points plotted are restricted to cases where the linear regression is a good fit to the overall profile. *Mean profiles* are the average of values taken from the rain rate-bin mean dBZ_{em} (11b) and the rain rate-bin mean gradient of dBZ_{em} (Fig. 10a).

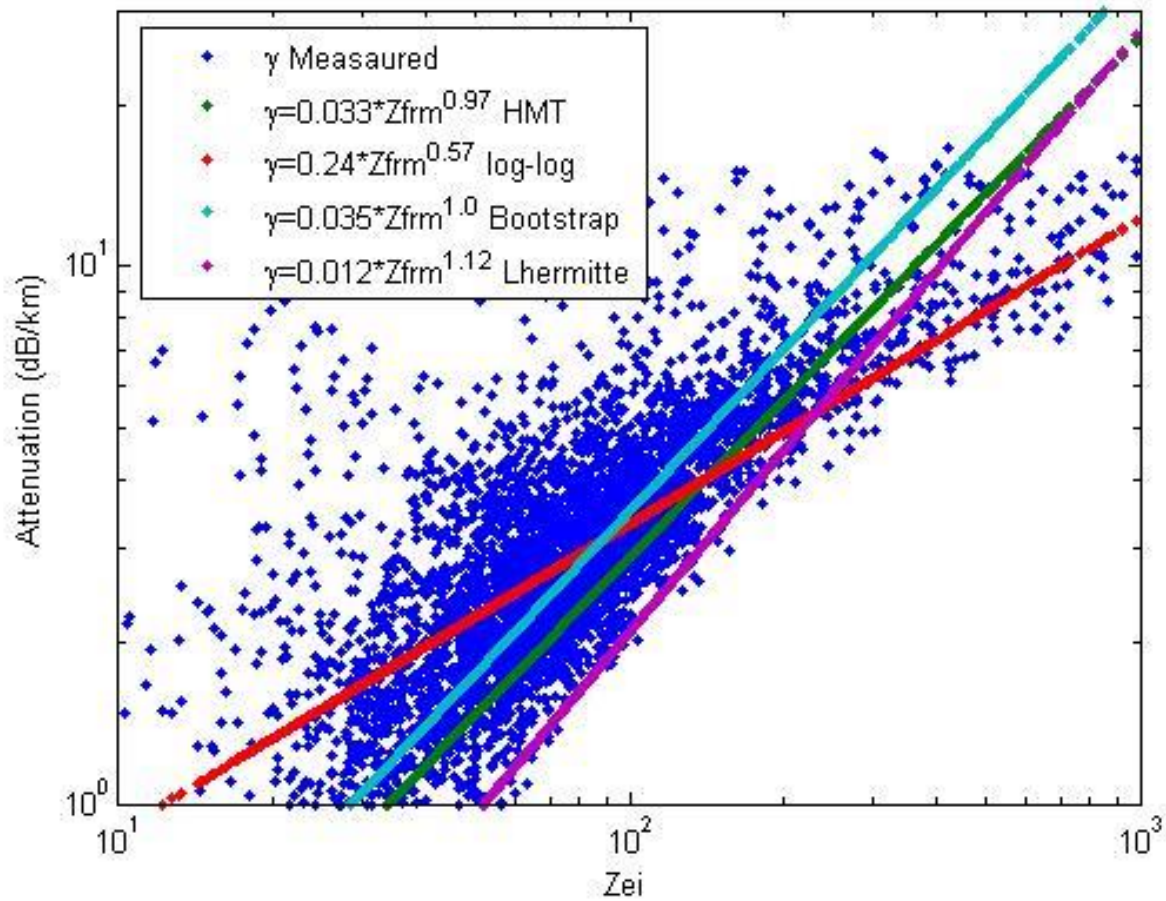

Figure 8. Results from analysis of each profile using regression fits of the form $dBZ_{em} = dBZ_{emi} + slope*h$ where attenuation vs Z_{emi} is shown. The lines are fits from Table 2 as shown above: green – HMT direct fit (line 6); red – log-log linear regression; cyan – bootstrap value (line 7): magenta – Lhermitte (line 1).

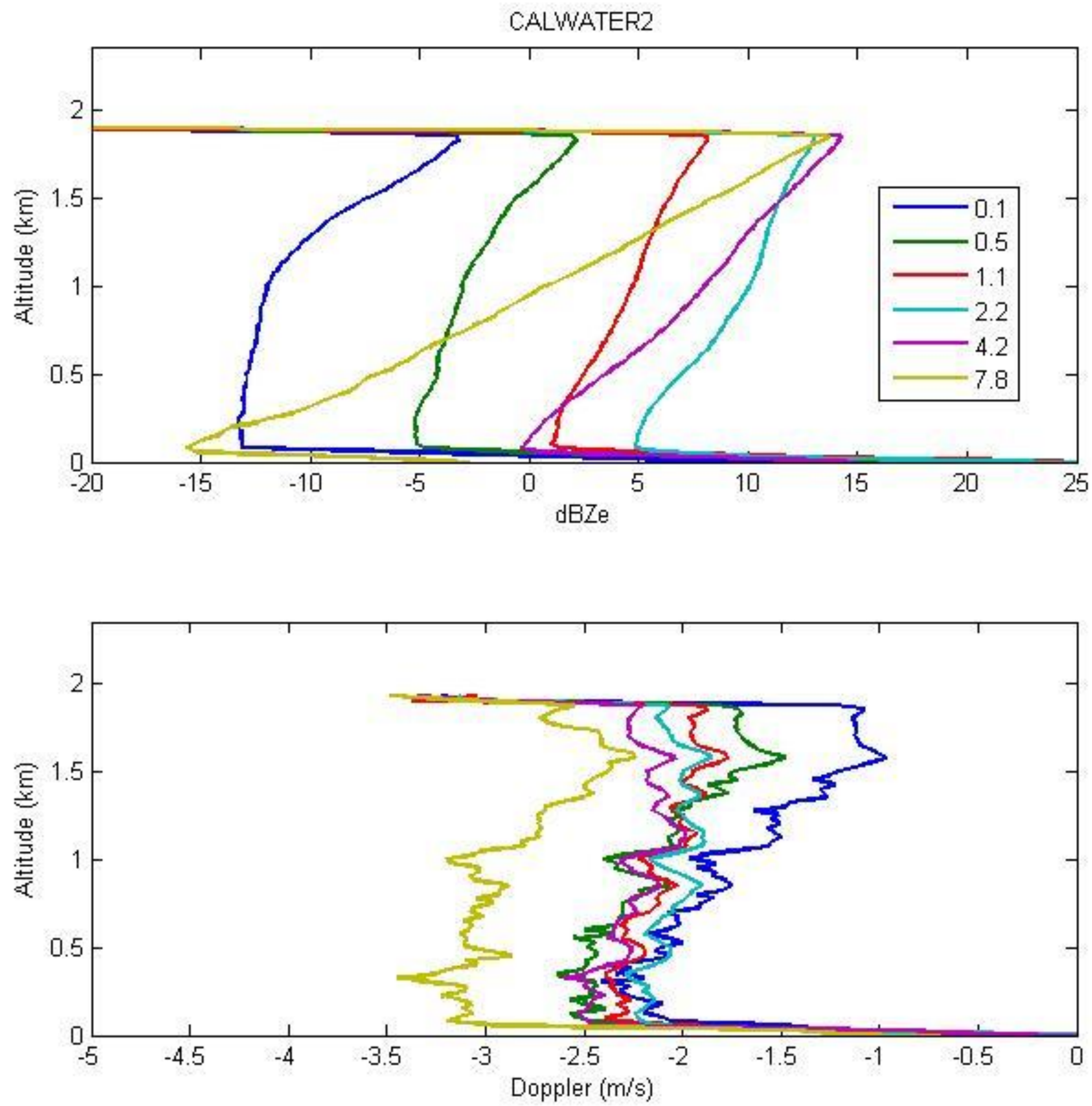

Figure 9. Profiles of bin-averages of dBZ_{em} (upper panel) and pitch-corrected Doppler vertical velocity (lower panel) for three hours on Feb. 05. The legend gives the mean rain rate in mm/hr for the bins. The bin edges for these results are rain rate = [0, 0.25, 0.7, 1.5, 3, 6, 13] mm/hr.

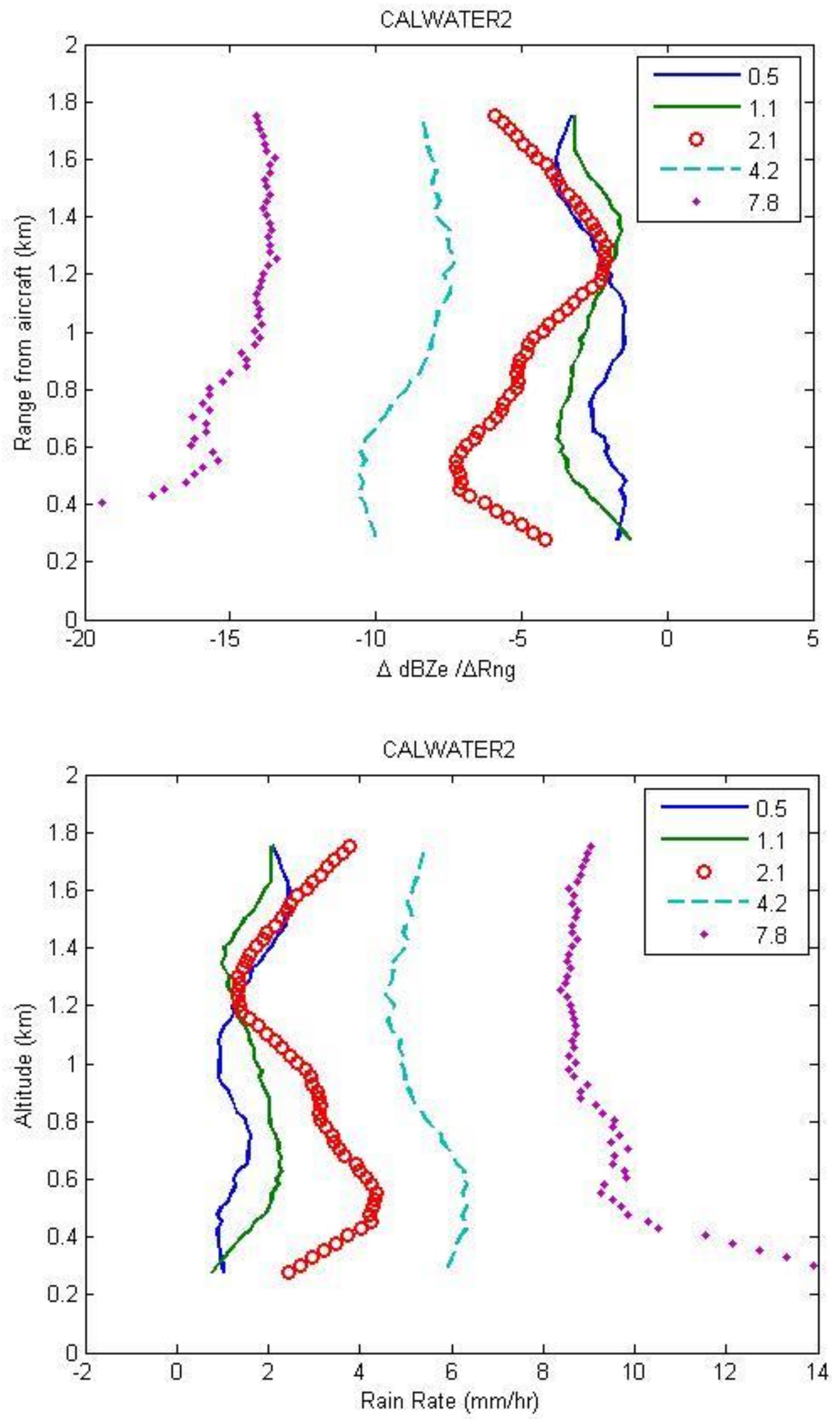

Figure 10. Rain rate-binned averaged profiles of dBZ_{em} slope (upper panel) and slope converted to rain rate (lower panel) using (9) and (11). The Upper panel is for when rain is present; the lower has the rainfree normalization.

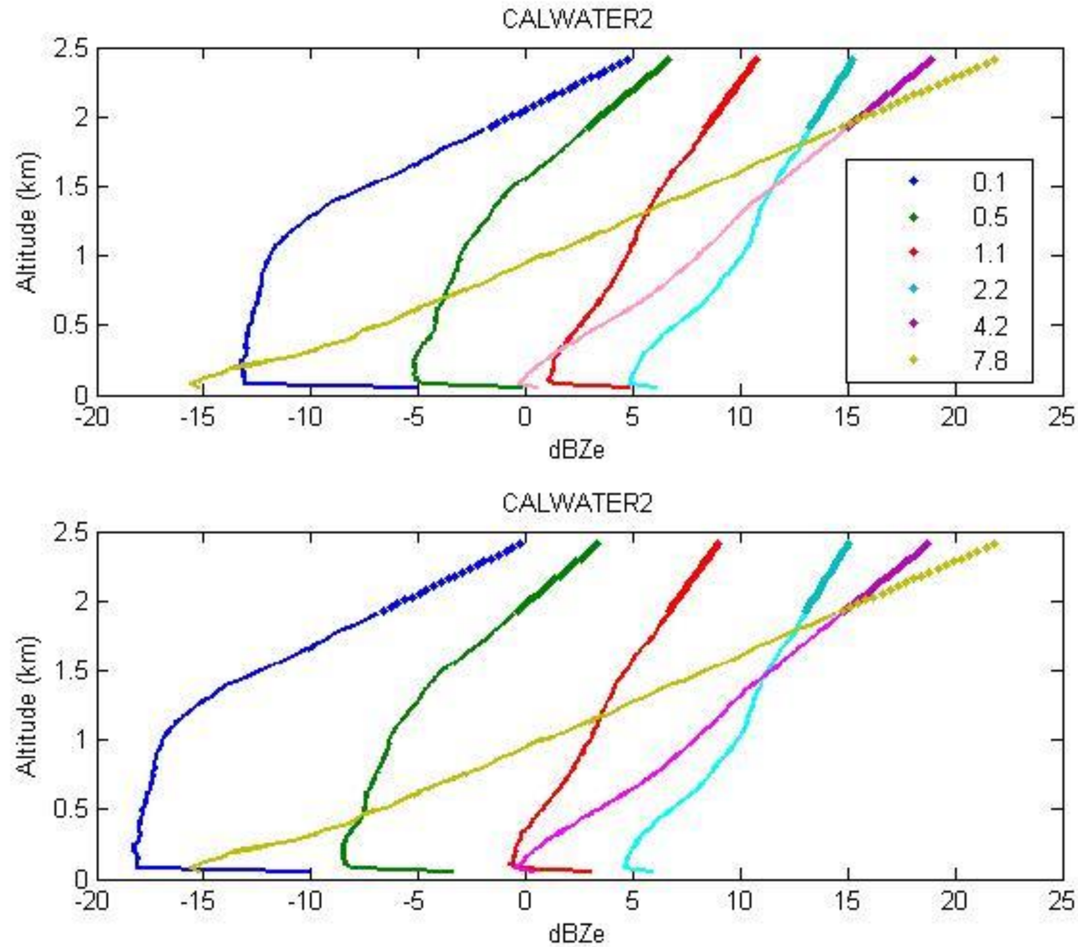

Figure 11. Mean dBZ_{em} profiles in bins of rain_nc. The upper panel is average dBZ_{em} when precipitation is present where we require $dBZ_{em}(4)-dBZ_{em}(75)>-5\ dB$. The lower panel is the same except the mean is multiplied by the fraction of profiles that meet the dBZ_{em} criterion to all profiles. The dotted portions of the profiles above 1.9 km are the extrapolations using the slope and intercepts.

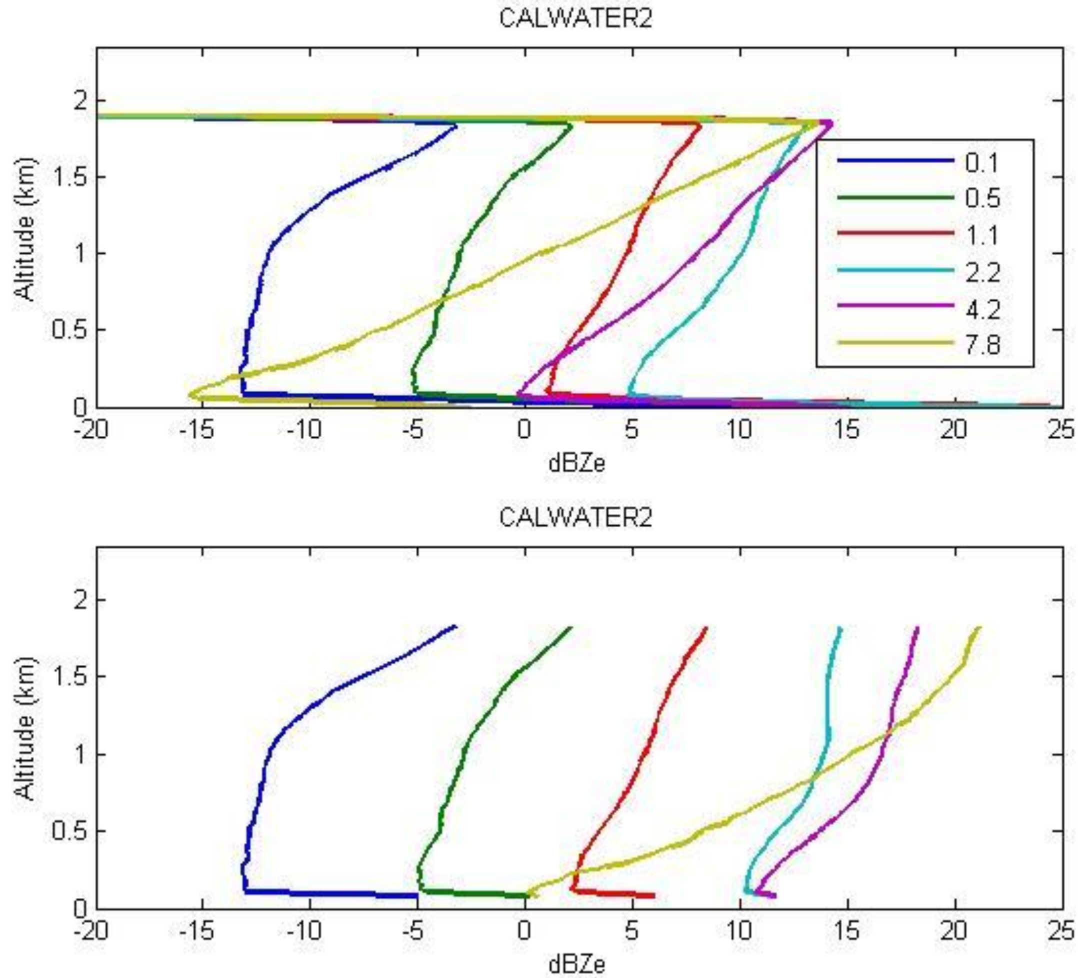

Figure 12. Profiles of mean dBZ_e (as per Fig. 10). The upper panel is raw mean dBZ_{em}; the lower panel is corrected using (18) with $\gamma_R = 0.05*Z_{em}^{1.0}$.

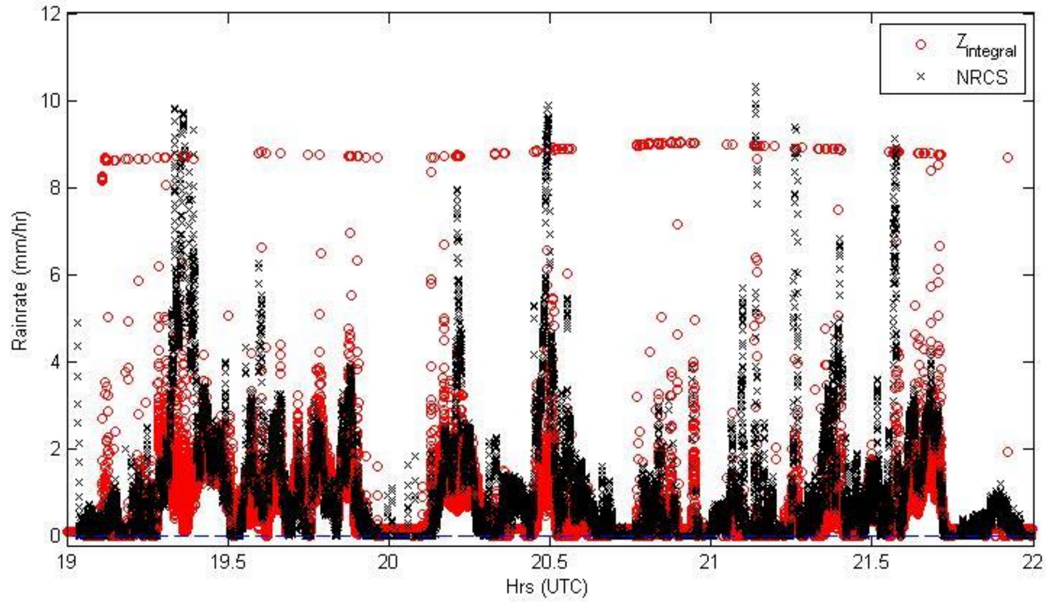

Figure 13. As in Fig. 6, but the Z-integral method is used to compute rain rate from attenuation, as per (21).